Desalination 329 (2013) 9–18

Contents lists available at ScienceDirect

Desalination

journal homepage: www.elsevier.com/locate/desal

Formation of thin film composite nanofiltration membrane: Effect of polysulfone substrate characteristics

N. Misdan [a,b], W.J. Lau [a,b], A.F. Ismail [a,b,*], T. Matsuura [a,c]

[a] Advanced Membrane Technology Research Centre (AMTEC), Universiti Teknologi Malaysia, 81310 Skudai, Johor, Malaysia
[b] Faculty of Petroleum and Renewable Energy Engineering, Universiti Teknologi Malaysia, 81310 Skudai, Johor, Malaysia
[c] Department of Chemical and Biological Engineering, Industrial Membrane Research Institute, University of Ottawa, 161 Louis Pasteur St., Ottawa, ON KIN 6N5, Canada

HIGHLIGHTS

- Properties of PSf substrate membranes were fundamentally investigated.
- Pore size and porosity of substrate portray major role in the changes of PA layer.
- TFC NF membrane made of PSf 15 wt.% substrate produced the best performance.

GRAPHICAL ABSTRACT

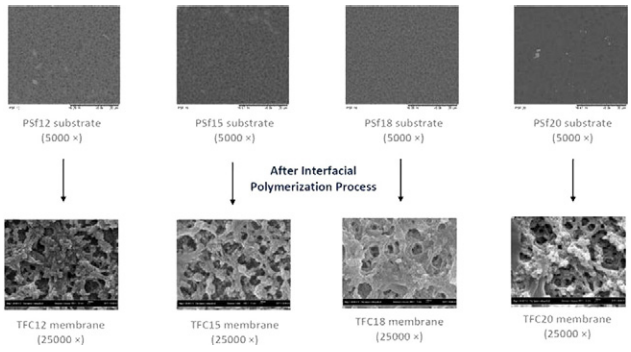

ARTICLE INFO

Article history:
Received 19 July 2013
Received in revised form 23 August 2013
Accepted 24 August 2013
Available online 23 September 2013

Keywords:
Nanofiltration
Thin film composite membrane
Substrate
Polysulfone
Water flux
Salt rejection

ABSTRACT

In this work, polysulfone (PSf) substrates with different properties were made by varying the polymer concentration in the dope solution in the range 12–20 wt.%. Polyamide (PA) thin layers were then formed via interfacial polymerization between piperazine and trimethylchloride over the PSf substrates. Both top PA thin layers and bottom PSf substrates were characterized with respect to physicochemical properties, structural morphology, and water flux/salt rejection to investigate the influence of substrate properties on the characteristics of PA thin layers. Physical properties of the PA layers were reported to be altered using different PSf substrate properties and were in good agreement with the change in water flux. From the FESEM pictures, it is found that the thickness of PA layer increased as the surface pore size of support membrane decreased. The change in the membrane structural properties in particular pore size is found to portray significant contribution to the changes of formed PA layer. Interestingly, only slight changes on Na_2SO_4 and $MgSO_4$ salt rejection were reported on any TFC membranes. Considering both water permeability and salt rejection rate, the best performing TFC membrane produced in this work was the membrane made over substrate of 15 wt.% PSf concentration.

1. Introduction

Since the first introduction in the early 1980s, nanofiltration (NF) membranes have attracted considerable industrial interest as a promising cost-effective material to the growing needs of separation and purification technologies. Considering that a NF membrane has a microporous

* Corresponding author at: Faculty of Petroleum and Renewable Energy Engineering, Universiti Teknologi Malaysia, 81310 Skudai, Johor, Malaysia. Tel.: +60 7 553 5592; fax: +60 7 558 1463.
E-mail addresses: afauzi@utm.my, fauzi.ismail@gmail.com (A.F. Ismail).

0011-9164/$ – see front matter © 2013 Elsevier B.V. All rights reserved.
http://dx.doi.org/10.1016/j.desal.2013.08.021

pore diameter (d_p) less than 2 nm, it is able to separate divalent and some monovalent ions, dissolved organic solutes (molecular weight M_w between 200 and 500 g/mol), hardness and heavy metals, effectively [1,2]. To date, thin film composite (TFC) membrane by far is the most commercially successful membrane for various industrial separation processes, particularly in the water treatment and purification applications [3–7]. The TFC membrane consists of an ultra-thin selective layer which is interfacially polymerized over a microporous substrate [8]. The main advantage of TFC membranes over asymmetric membranes is that each layer can be independently optimized to attain desired permeability and selectivity.

Up to now, various parametric studies have been conducted in an attempt to develop high performance TFC membranes by optimizing mainly the top thin selective layer. Physical and chemical properties of the substrate, however, are paid less attention during TFC membrane fabrication, probably because the substrate plays no significant role in the solute separation and fouling reduction as the top selective layer does [9]. The impact of substrate properties of the composite membrane formation is, therefore, less reported in the open literature during the preparation of TFC membranes. In view of the importance of a substrate to the formation of a composite membrane, several studies have been done in the past recent years to investigate the correlation between substrates made of different properties and the properties of ultrathin polyamide (PA) selective layer [10–12]. It is believed that the morphology (i.e. structure, thickness and surface charge) and the performance (i.e. permeability and selectivity) of a TFC membrane may be altered with the use of different substrate properties [6,12,13].

In 2006, Singh et al. [10] revealed that the change in pore size distribution of the polysulfone (PSf) substrate could affect the formation of a reverse osmosis TFC membrane and its performance as well. Smaller pores of PSf substrates (<70 nm) exhibited a tremendous salt rejection efficiency to that of bigger pores (>150 nm). This is mainly due to a notable increase in effective layer thickness caused by the smaller pores which restrict the penetration of PA into those pores. Years later, another extensive study was also conducted by Ghosh and Hoek [12] to investigate the impact of PSf support properties on the formation of composite membranes. It explained that the variance in the physical structure and chemistry of a PSf substrate apparently produced a PA with different characteristics and performance.

In particular, the polymer concentration in the substrate casting solution is believed to be one of the primary factors influencing the physical characteristics of the substrate. Moreover, the polymer concentrations in the casting solution are found to be above 12 and below 20 wt.%, and mostly in the range of 15 to 18 wt.% [6,12,14–17]. Therefore, it is our intention to investigate the relationship between the physical properties of substrate (i.e. surface pore size, pore size distribution and surface porosity), made of different polymer concentrations (in the range of 12–20 wt.%), and the characteristic of NF composite membrane. It is generally known that each substrate possesses its own characteristics. Therefore, the support layer itself has to form a good agreement between pore size and high flux to diminish the additional resistance for water transport. However, to what extent would the pore structure eventually influence the composite membrane fabrication still remains unclear. In order to gain further insights and to achieve the objective of the present study, topographical images of each substrate surface will be further recorded by SEM and AFM following quantitative measurements described by previous studies. Thus, the obtained values from both characterizations will be discussed in detail. It should be noted that optimized conditions of PA layers, including monomer concentration, reaction time, curing temperature and time, or the addition of additives, during the TFC membrane preparation is not conducted in this study. It is expected that the findings from this work would provide more insight in TFC membrane fabrication which can be generally optimized through the top PA active layer and bottom substrate layer.

2. Experimental

2.1. Materials

Polysulfone (Udel® P-1700) purchased from Solvay Specialty Polymers, USA was used to fabricate substrate for TFC membrane. PSf (in pellet form) was first dried at 100 °C overnight prior to use. Polyvinylpyrrolidone (PVP) K30 of M_w 40,000 used as a pore forming agent during substrate fabrication was purchased from Fluka Chemie GmbH, Switzerland. Trimethylchloride (TMC) and piperazine (PIP) were purchased from Sigma-Aldrich and Merck, respectively and were used to establish the PA layer on PSf substrate. 1-Methyl-2pyrrolidone (purity > 99.5%) and n-Hexane supplied from Merck were used without further purification. Na_2SO_4 and $MgSO_4$ supplied by GCE Laboratory Chemicals were used to prepare aqueous salt solution for membrane flux and rejection determination.

2.2. Membrane preparation

2.2.1. Preparation of PSf substrate

Asymmetric PSf substrates were prepared via phase inversion technique using the dope formulations as shown in Table 1. In order to increase the porosity of PSf substrates, 1 wt.% PVP was added into dope solution and acted as a pore forming agent. To prepare the dope solution, PVP was first dissolved in NMP solvent followed by PSf. The dope solution was stirred continuously until a homogeneous polymer solution was obtained. The substrate was then cast on a glass plate using the dope solution prepared. The cast substrate was kept for 30 s at ambient temperature before immersing into a water coagulation bath at room temperature. Obtained microporous PSf support was washed thoroughly with de-ionized water to remove residual solvent followed by keeping wet at 5 °C prior to use. The substrates prepared were denoted as PSf 12, PSf 15, PSf 18 and PSf 20, respectively, where the number corresponded to the PSf concentration used in the dope solution.

2.2.2. Preparation of thin-film composite (TFC) NF membrane

TFC NF membranes were prepared via in-situ interfacial polymerization process between PIP and TMC as shown in Scheme 1. PSf substrate was initially taped onto the glass plate followed by 120 s of immersion in an aqueous solution of 2% (w/v) PIP. The excess solution from the impregnated membrane surface was eliminated using a soft rubber roller. The membrane was then immediately immersed into the *n*-hexane solution of 0.2% (w/v) TMC for 60 s, which resulted in in-situ formation of an ultra-thin PA layer over the microporous PSf substrate. Subsequently, the resulting membrane was cured at 60 °C for 5 min and finally was thoroughly washed with de-ionized water before storage in de-ionized water at 5 °C prior to use. The composite NF membranes prepared were then denoted as TFC 12, TFC 15, TFC 18 and TFC 20, respectively, where the number corresponded to the PSf concentration used in preparing the substrate.

2.2.3. TFC NF membrane performance evaluation

The flux and rejection of fabricated TFC NF membranes were analyzed using a dead-end filtration system (Sterlitech™ HP4750 Stirred Cell) under a nitrogen atmosphere. TFC membranes were initially compacted at a trans-membrane pressure of 0.8 MPa with DI water

Table 1
Dope formulation used to prepare different types of substrates.

Substrate	Dope formulation (wt.%)		
	PSf	PVP	NMP
PSf 12	12	1	87
PSf 15	15	1	84
PSf 18	18	1	81
PSf 20	20	1	79

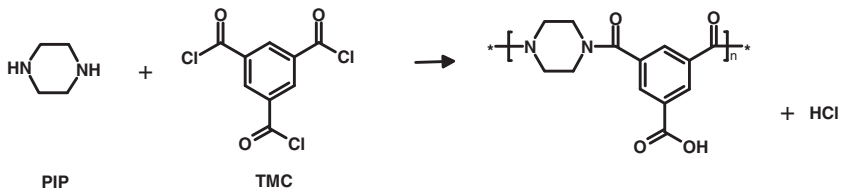

Scheme 1. Interfacial polymerization of poly(piperaizine-amide).

for about 1 h. The active membrane surface area was 14.6 cm^2. The NF experiments were then performed using 1000 ppm Na_2SO_4 (or $MgSO_4$) solution at operating pressure and temperature set at 0.5 MPa and 25 °C, respectively. Membrane water flux (F) was subsequently measured using the following equation:

$$F = \frac{V}{t \times A} \tag{1}$$

where V is the permeate volume (L), A is the membrane area (m^2) and t is the experimental time to obtain V (h).

A bench conductivity meter (Jenway 4520) was used to measure the salt concentration in the feed and permeate solutions. The membrane salt rejection was then determined using the following equation:

$$R(\%) = \left(1 - \frac{C_p}{C_f}\right) \times 100 \tag{2}$$

where, C_p is the permeate concentration (ppm) and C_f is the feed concentration (ppm), respectively.

2.3. Substrate and PA layer characterization

The chemical structure of membranes prepared was characterized using an FTIR spectrometers FTLA2000 (ABB, Switzerland) equipped with an attenuated total reflection (ATR) supplied by the PIKE MIRacle™ (USA). A total of 128 scans were measured during IR studies for each sample. The apparatus resolution was 8 cm^{-1}.

The water contact angle (CA) was measured using a Phoenix 300 contact angle analyzer (S.E.O. Co., Ltd, Korea). Ten drops of de-ionized water were measured for each sample at room temperature. The average of measured contact angle was reported as the CA value of the membranes. The surface roughness corrected solid–liquid interfacial free energy, $-\Delta G_{SL}$, was estimated using a method as described in a previous study [18]. The $-\Delta G_{SL}$ can be estimated using the following equation:

$$-\Delta GSL = \gamma L\left(1 + \frac{\cos\theta}{\Delta}\right) \tag{3}$$

where, θ is the average contact angle value, Δ is the relative surface area and $\gamma_L = 72.8$ mJ/m^2 (for pure water at 25 °C) is the liquid surface tension, respectively. For a smooth surface, the maximal solid–liquid interfacial free energy is $2\gamma_L$ as contact angle is 0°. Subsequently, the higher value of $-\Delta G_{SL}$ indicates an increased hydrophilicity of the surface.

The top surface and cross-sectional morphologies of composite membranes were visualized using field emission scanning electron microscope (FESEM) (JEOL JSM-6700F). The samples were fractured in liquid nitrogen and dried under vacuum. Subsequently, membranes were sputter-coated with gold to prevent charging. Additionally, mean pore size (dp_{avg}) and surface porosity (ε) of PSf substrates made of different polymer concentrations were evaluated using ImageJ software developed by the National Institute of Health (NIH) on the membrane SEM surface images. The FESEM surface images were binarized at a certain threshold in order to obtain a clear image of membrane surface pores following a procedure described in previous studies [19–21].

Atomic force microscopy (AFM) (Multimode 8 AFM instrument equipped with a NanoScope V controller) was used to characterize the surface morphology of the membranes in terms of mean roughness parameter and pore sizes (i.e. mean pore size, geometric standard deviation and pore size distribution). The scanning area of each membrane was 5 μm × 5 μm. The pore sizes and the probability density function curves of the substrates were determined using a previous method described by several authors [22–24].

3. Results and discussion

3.1. Effect of polymer concentration on PSf substrate properties

3.1.1. Organic functional groups

The chemical property of substrates was analyzed using an ATR-IR spectroscopy. Fig. 1 shows the IR spectra of the four PSf substrates prepared. IR bands at 1323 cm^{-1}, 1292 cm^{-1}, 1242 cm^{-1} and 1149 cm^{-1} were the typical characteristic peaks of the substrate made of PSf. A broad transmittance band at 1670 cm^{-1} which corresponded to C O stretching could indicate the presence of PVP additive in the substrate matrix. The remaining PVP entrapped in substrate also revealed that the polymeric additive had not completely leached out during phase inversion and would therefore play a role in improving substrate hydrophilicity. Overall, the chemical property of all substrates remained the same irrespective of polymer concentration used.

3.1.2. Surface morphology (FESEM)

Fig. 2 presents the FESEM image of top surface of each PSf substrate made. It is seen that the pores of PSf 12, PSf 15 and PSf 18 substrates were evenly distributed throughout the substrate surface and could be easily observed when examined at a magnification of 5000×. Due to the decrease in pore size on PSf 20 substrate, these pores were unable

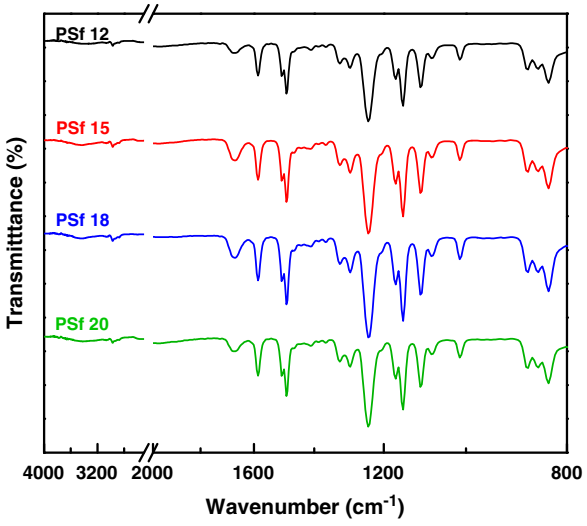

Fig. 1. ATIR-IR spectra of PSf substrates made of different polymer concentrations.

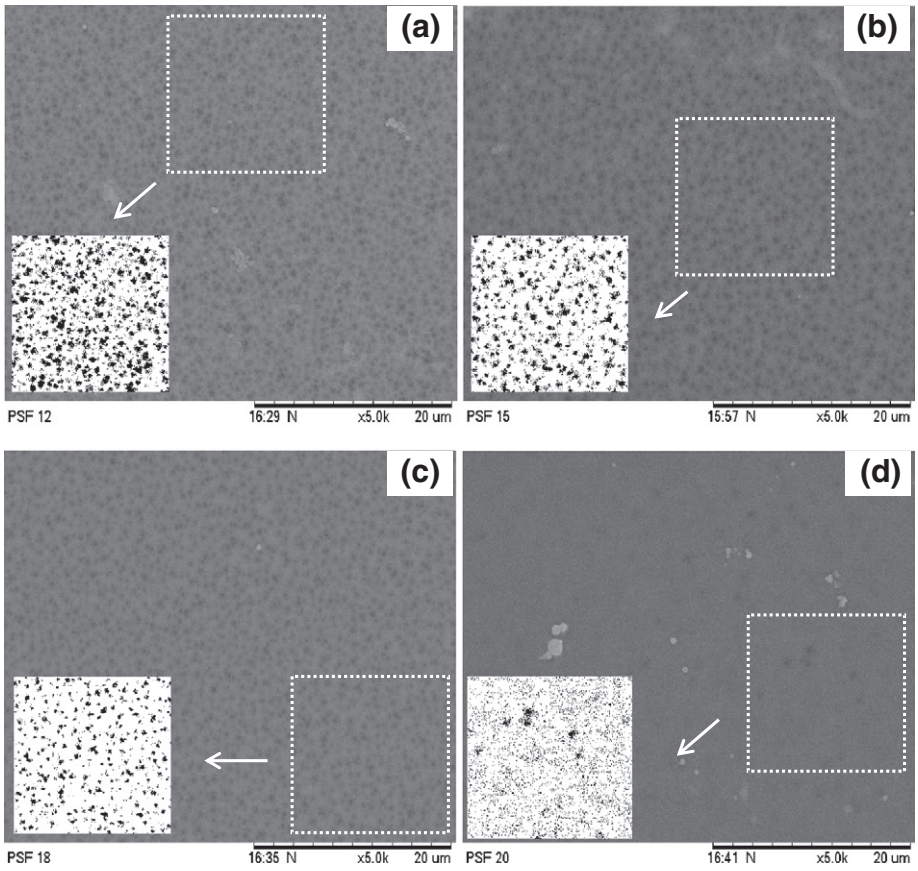

Fig. 2. FESEM images of top surface of PSf substrates, a) PSf 12, (b) PSf 15, (c) PSf 18 and (d) PSf 20. (Note: threshold image placed on the bottom left corner of each SEM image was used to determine the average pore size and porosity of PSf substrate).

to be seen at the same magnification. To evaluate the effect of polymer concentration on the substrates' average pore diameter (dp_{avg}) and porosity (ε), Image J software was employed. A specific area of the surface on gray-scale SEM image was selected to convert to a black and white image which the black small spots represented the pores on the substrate surface. The average pore diameter values were then computed and the data are tabulated in Table 2. As expected, the pore size of substrate decreased with increasing polymer concentration. The decrease in pore diameter of PSf 12 substrate from 84 nm to <12 nm in PSf 20 substrate could be explained by the delayed solvent (NMP) and non-solvent (water from the coagulation bath) exchange rate during the phase inversion process which resulted from higher viscosity of dope solution used. In addition to the pore size change, it is also reported that substrate surface porosity was altered with the use of different polymer concentrations. The computed surface porosity decreased according to PSf 12 (23.04%) > PSf 15 (11.97%) > PSf 20 (10.06%) > PSf 18 (5.78%). For the PSf 12, PSf 15 and PSf 18 substrates, the results shown were in a good agreement with a previously reported study where the % surface porosity was inversely proportional with the surface pore size of substrate [10]. It is noted that PSf 20 displayed higher surface porosity than that of PSf 18 and this may be an error which could be caused by pores covered (resulted in size diminution) by coating element during sputter-coating process.

Table 2
The mean pore size (μ_p), geometric standard deviation (σ_p), average pore diameter (dp_{avg}) and surface porosity (ε) of PSf substrates prepared from different polymer concentrations.

Substrate	AFM measurement		SEM measurement	
	μ_p (nm)	σ_p (nm)	dp_{avg} (nm)	ε (%)
PSf 12	86.19	1.34	84.40	23.04
PSf 15	53.20	1.31	47.20	11.97
PSf 18	41.07	1.35	38.40	5.78
PSf 20	38.24	1.43	11.70	10.06

3.1.3. Surface roughness (AFM)

Fig. 3 shows the AFM topographic images together with roughness values of PSf substrates made of different polymer concentrations. As can be seen, the surface roughness of PSf substrate was reduced with an increase in polymer concentration, indicating smaller surface pore sizes tended to create a smoother surface on a PSf substrate. The correlations between surface roughness and membrane pore structure have also been previously reported [22,24,25]. Using the AFM image analysis program, the pore dimension of all PSf substrates was quantitatively determined based on a scanning surface area of 2 μm × 2 μm. The mean pore sizes μ_p and the geometric standard deviations σ_p of the substrates as shown in Table 2 were determined using a previously stated procedure [22–24]. The probability density function curve of each PSf substrate made is also presented in Fig. 4 in which the curves were clearly seen to be shifted to the left with increasing polymer concentration, indicating the decrease in substrate pore size. Comparisons made between the pore size obtained from AFM images and FESEM images showed the same decreasing pore size trend (with increasing polymer concentration), but the pore size determined from the AFM image was bigger. This is mainly because of the diminution of pore sizes due to a coating procedure that is generally required for FESEM characterization [24,26].

3.1.4. Water flux and surface hydrophilicity

With respect to water flux and surface hydrophilicity, it is also found that both properties were influenced by the polymer concentration used in preparing substrates. Table 3 shows effect of PSf concentration

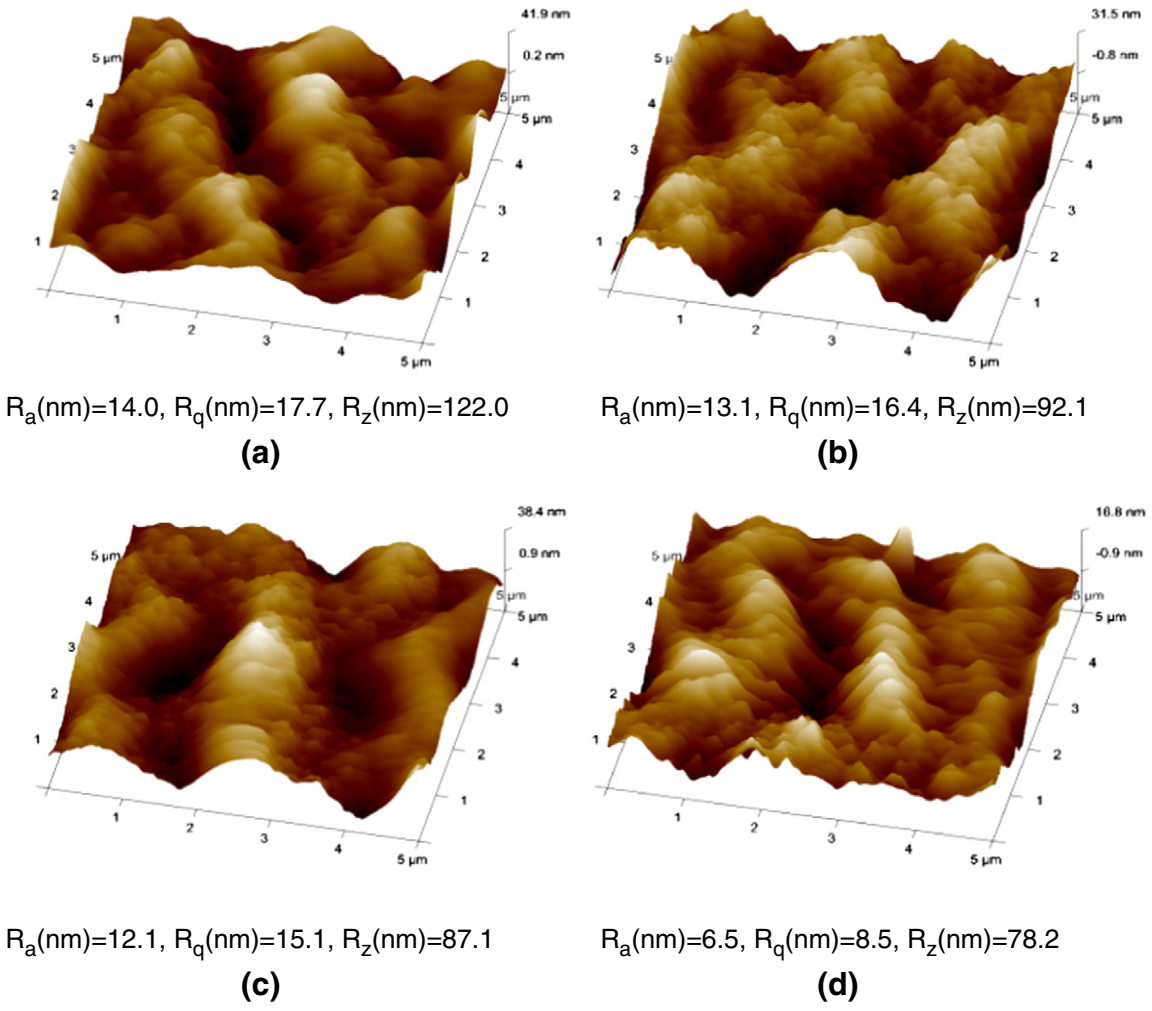

Fig. 3. 3D AFM images of PSf substrates together with surface roughness values, (a) PSf 12, (b) PSf 15, (c) PSf 18 and (d) PSf 20.

on the substrate properties with respect to pure water permeability, contact angle and the surface area corrected interfacial free energy ($-\Delta G_{SL}$). Owing to the decrease in substrate pore size as discussed in the previous section (Section 3.1.2), the decrease in water flux of PSf 20 substrate to 20.3 from 683.1 L/m^2·h·bar reported in PSf 12 substrate was reasonable and followed the trend of change. The water contact angle on the other hand was found to increase slightly from 66.3° to 70.8° with increasing PSf concentration from 12 to 20 wt.%. The small increase in contact angle value could not be used to show the increased hydrophobicity of substrate as the substrate surface roughness might also contribute to the change of contact angle value [18,27]. Therefore, instead of contact angle value, $-\Delta G_{SL}$ was considered as a better determination of surface hydrophilicity. Results showed that the degree of surface hydrophilicity reduced (lower $-\Delta G_{SL}$ value) with increasing polymer concentration, revealing that the flux reduction in substrate could also be due to the decrease in surface hydrophilicity in addition to pore dimension and surface roughness.

Based on the characterization on the substrate properties, it is hypothesized that the properties of TFC membranes could be altered

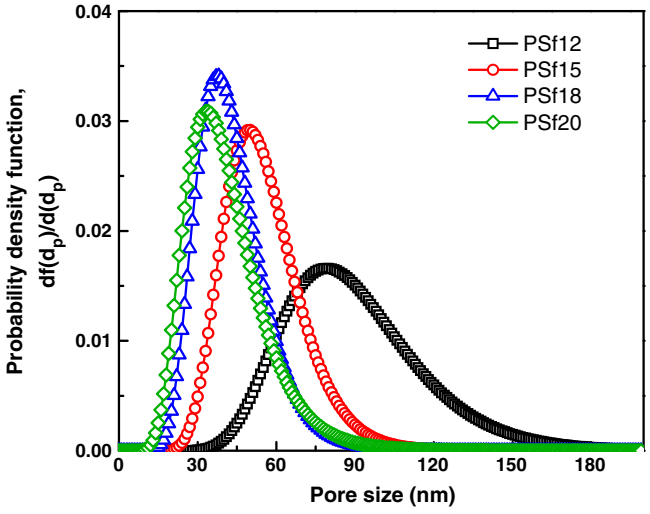

Fig. 4. Probability density function curves of different PSf substrates.

Table 3
Properties of substrates with respect to pure water permeability, contact angle and $-\Delta G_{SL}$.

Substrate	Pure water permeability (L/m^2·h·bar)	Contact angle (°)	$-\Delta G_{SL}$ (mJ/m^2)
PSf 12	683.1	66.3 ± 1.1	102.0
PSf 15	220.0	67.7 ± 1.4	100.3
PSf 18	61.8	69.8 ± 1.3	97.9
PSf 20	20.3	70.8 ± 1.7	96.6

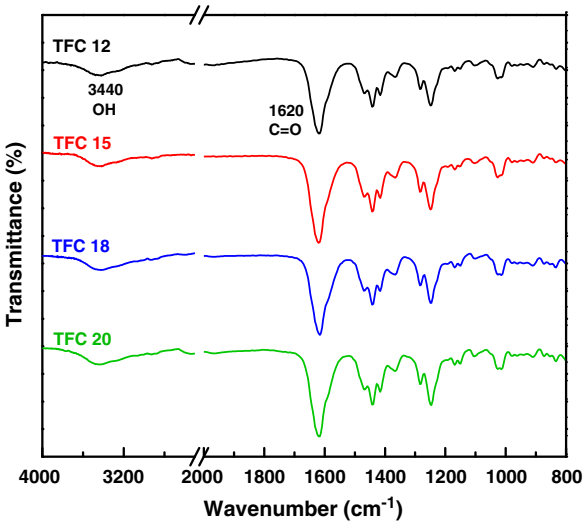

Fig. 5. ATR-IR spectra of TFC NF membranes prepared over different PSf substrates.

using PSf substrates of different properties (e.g. pore size, surface porosity, surface roughness and hydrophilicity). In the following section, we will investigate to what extent the changes in substrate properties would affect the characteristics of PA layer formation and further the performance of TFC NF membrane during the filtration process.

3.2. Effect of polymer concentration on TFC NF membrane properties

3.2.1. Organic functional groups of PA layer

Fig. 5 shows the IR spectra of the polyamide TFC membranes prepared from different substrate properties. The IR spectra indicated that the interfacial polymerization between PIP and TMC was successfully formed over all PSf substrates owing to the presence of strong band at 1620 cm^{-1}. This peak was corresponded to the C O band of an amide group. In addition, a broad band found at 3440 cm^{-1} could be assigned to the presence of –COOH groups formed in PA thin layer. The appearance of carboxylic acid functional groups is attributed to the partial hydrolysis of the acyl chloride unit of TMC [28]. Overall, the IR spectra revealed that PA layer could still be established even though there was a significant change in substrate properties, particularly the pore size of the substrate.

3.2.2. Surface roughness and morphology of PA layer

The surface roughness of TFC membranes was characterized using AFM analysis and the 3D topographic together with roughness values is presented in Fig. 6. Compared to the surface roughness of PSf substrates (see Fig. 3), the significant increase in surface roughness on composite membranes was well-matched with the typical ridge-valley structure of

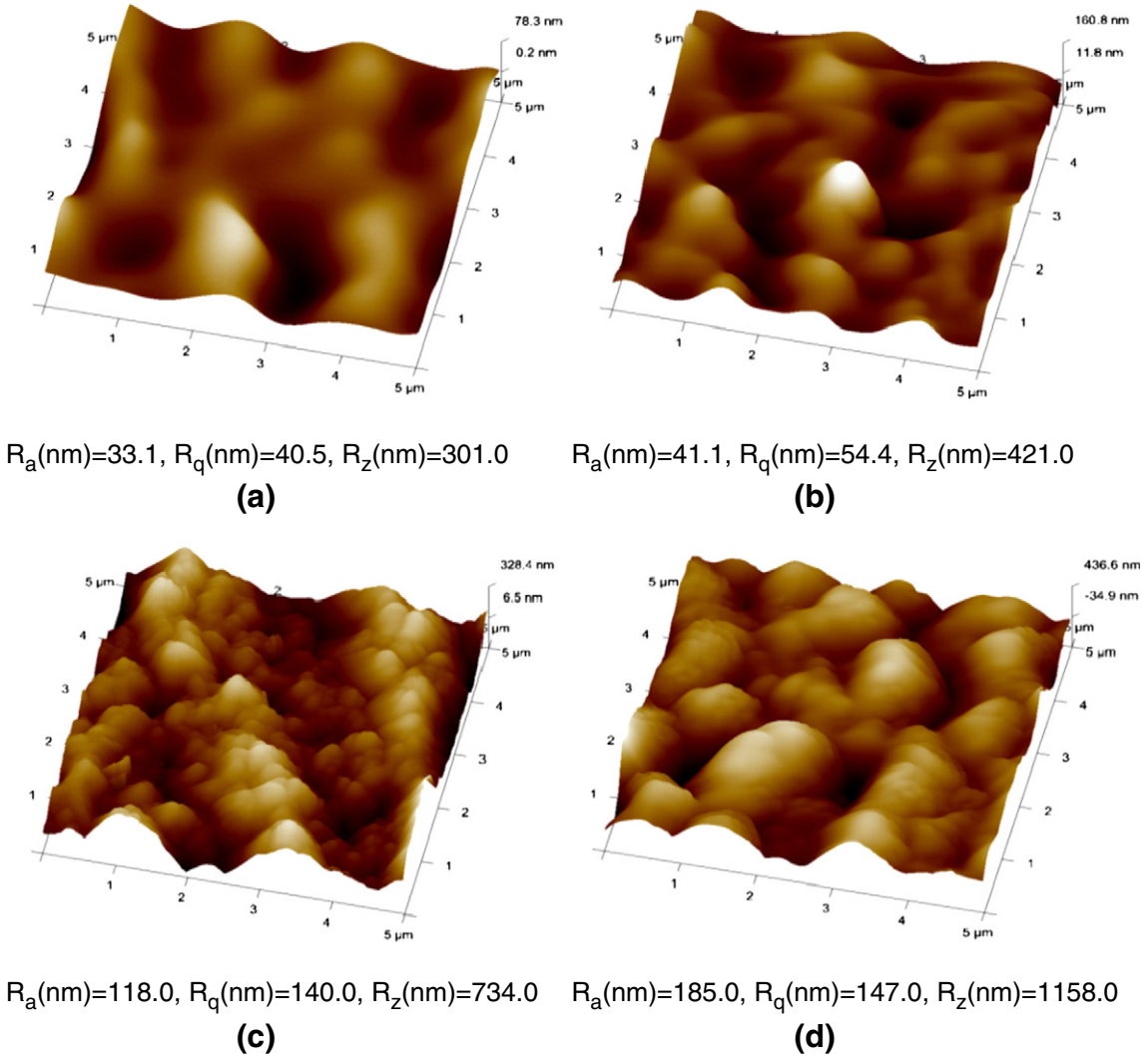

R_a(nm)=33.1, R_q(nm)=40.5, R_z(nm)=301.0 **(a)**

R_a(nm)=41.1, R_q(nm)=54.4, R_z(nm)=421.0 **(b)**

R_a(nm)=118.0, R_q(nm)=140.0, R_z(nm)=734.0 **(c)**

R_a(nm)=185.0, R_q(nm)=147.0, R_z(nm)=1158.0 **(d)**

Fig. 6. 3D AFM images of TFC NF membranes together with surface roughness values, (a) TFC 12, (b) TFC 15, (c) TFC 18 and (d) TFC 20.

PA layers. Though the roughness of PSf substrate decreased with increasing polymer concentration, the roughness of TFC membranes prepared showed the opposite trend in which TFC 20 membrane displayed the highest roughness value while TFC 12 membrane the lowest. In view of this, it is fair to say that substrate roughness might not be the main factor governing the changes in TFC surface roughness.

Representative FESEM top surface and cross-sectional images of TFC membranes are also presented in Figs. 7 and 8, respectively. In the images of the top surface, the white parts represented the peaks while the dark areas corresponded to the valleys. The variation in the surface morphology of TFC membrane compared to the PSf substrate confirmed that PA active layer was successfully formed over PSf substrate. Clearly, there was a change in PA layer structure with the use of different substrate properties. The TFC 12 and TFC 15 membranes prepared from low polymer concentration substrates exhibited uniformly formed "ridge-and-valley" like structure. Further increases in the polymer concentration of substrate tended to cover the valley film, increasing the ridge portion of PA layer as evidenced in TFC 18 membrane. This, as a consequence, resulted in the increase in PA layer thickness as evidenced on the cross-sectional image of the membrane. For TFC 20 membrane, it is believed that the nodular structures drawn as white circles in Fig. 8 (d) resulted from the tight pore structure of the substrate used. The

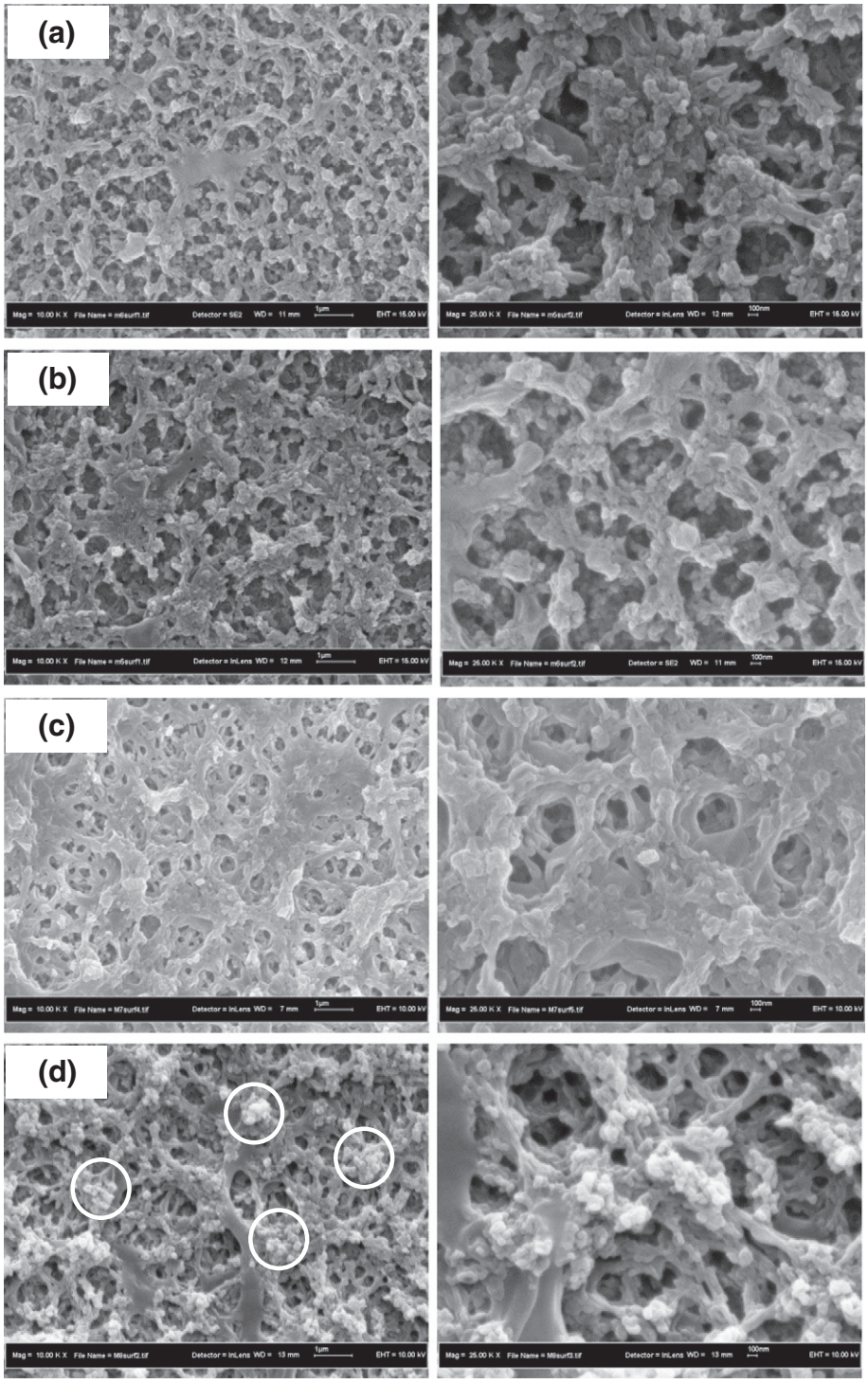

Fig. 7. FESEM images (left — 10,000× and right — 25,000×) of top surfaces of TFC NF membranes prepared from different PSf substrates, (a) TFC 12, (b) TFC 15, (c) TFC 18 and (d) TFC 20.

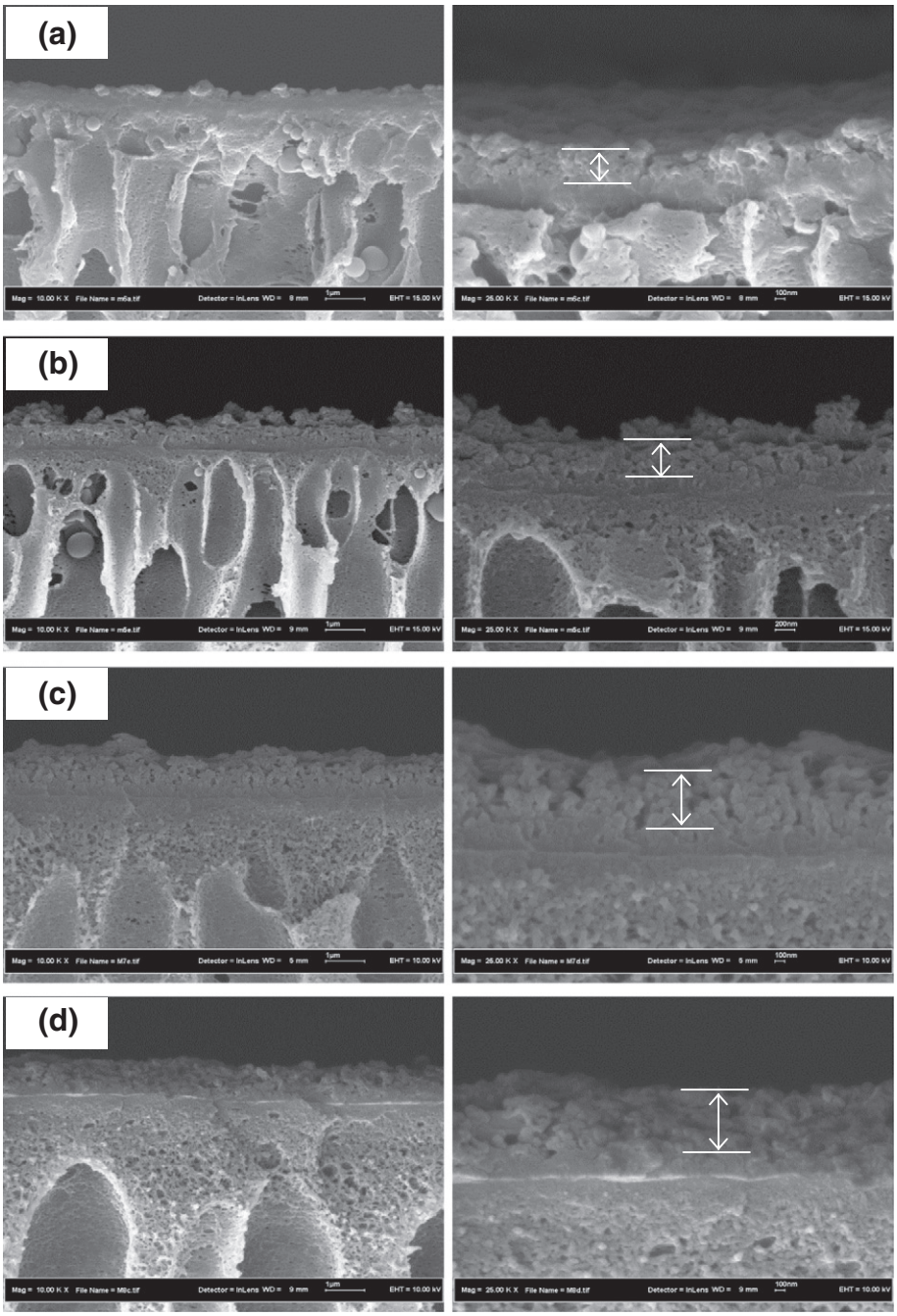

Fig. 8. FESEM images (Left — 10,000× and right — 25,000×) of cross-sectional morphologies of TFC NF membranes prepared from different PSf substrates, (a) TFC 12, (b) TFC 15, (c) TFC 18 and (d) TFC 20.

existence of these nodular structures gave quantitatively rougher surface morphology and increased PA layer thickness which is consistent with the AFM analysis and FESEM analysis, respectively. It must be pointed out that the irregular morphology of PA layer would preclude precise quantification of the layer thickness. Nevertheless, based on the cross-sectional images captured at a magnification of 25,000×, it can be seen that there was a significant increase in PA layer thickness with increasing substrate's polymer concentration. The variation of PA layer thickness can be explained by the fact that bigger pores of substrate would allow the PIP aqueous solution to diffuse deep into the pore channel, leading to the possibility of PA cross-linking inside the pores. On the other hand, smaller pores would limit the diffusion of PIP aqueous solution deep into the pores, developing thicker PA layer and greater surface roughness as evidenced in the work of Singh et. al [10]. Yet another interpretation is on the assumption that PIP is supplied to the organic and aqueous phase interface by the diffusion through the pores of the substrate skin layer from the pool of the aqueous phase in the porous sublayer, and this is the rate controlling step for the PIP supply. Unlike pressure-driven filtration, the PIP supply rate should be proportional to the effective porosity of the substrate membrane, ε/δ, where ε and δ are the porosity and thickness of the substrate skin layer, respectively. The ratio of ε/δ of PSf 20 membrane to that of PSf 12 membrane can be easily calculated by applying the Poiseuille equation to the measured pore size and the pure water permeation flux of the respective membranes, and the result is 1.54. This value is close to the thickness ratio (~1.8) of PSf 20 to PSf 12 membrane. Interestingly, the decrease in the pore size results in the more quick supply of PIP to the interface, and hence the increase in the PA layer thickness, due to the decrease in δ.

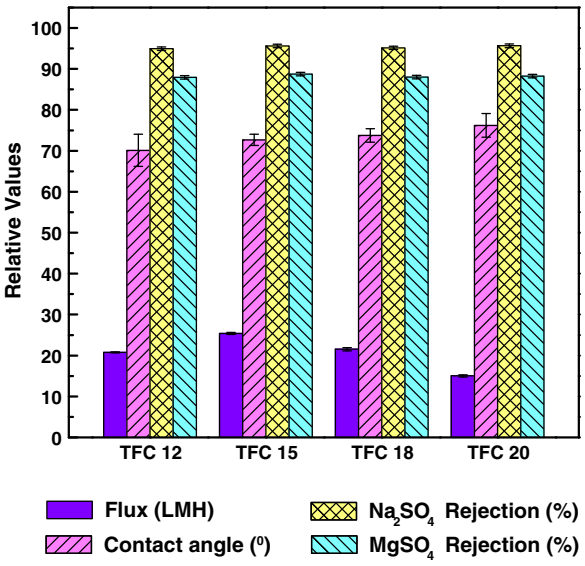

Fig. 9. Water flux and salt separation rate of TFC NF membranes made of different PSf substrates.

3.2.3. Water flux and salt rejection

Experimental data of flux, salt rejections and water contact angle of TFC membranes are outlined in Fig. 9. The error bars indicated the standard deviations of average measured values. With respect to water flux, it is reported that the flux decreased in the order of TFC 15 > TFC 18 ≥ TFC 12 > TFC 20. These results obtained were mainly influenced by the varied morphology of PA layer formed over the different PSf substrates. The lowest flux reported in TFC 20 membrane is most likely due to the significant increase in PA selective layer thickness, creating additional resistance for water transport through the membrane. An increase in ridge portion as found in TFC 18 membrane could also be the reason lowering the flux of the prepared membrane. Though TFC 12 and TFC 15 membranes exhibited very similar "ridge-and-valley" like structure, the water flux shown by each membrane was quite different. This may be explained by the formation of PA layer inside the pores as have been discussed in the previous section (Section 3.2.2), resulting in a drop in water permeation rate.

Comparing Na_2SO_4 (with monovalent cation) rejection with $MgSO_4$ (with divalent cation), the former is higher than the latter, indicating the presence of residual –COCl functional groups in the TMC monomer that are unreacted for cross-linking during IP process. These COCls are later hydrolyzed to COOHs in aqueous solution which give negative charge to the membrane, causing the rejection of Na_2SO_4 higher than $MgSO_4$. Overall, based on the AFM and FESEM analysis, we are convinced that the physical characteristics of PA layer e.g. layer thickness and surface roughness could be obviously altered using different substrate properties which, as a result, affected the water permeation rate. It must be emphasized that the findings obtained in this study might differ if the substrate is made of another type of polymer and/or with the presence of other additives. Thus, the results shown here were based on the observations on substrates made of commonly used PSf with the mean pore size in the range 38–86 nm (based on AFM analysis), water contact angle between 66 and 70°, R_a value of 6.5–14 nm and water flux of 20–680 $L/m^2 \cdot h \cdot bar$.

4. Conclusions

The correlation between the poly(piperazine-amide) layer and the underlying PSf substrate was fundamentally investigated on TFC NF membranes. PSf substrates with different properties were prepared by varying the concentration of polymer in the dope solution ranging from 12 to 20 wt.%. Among the parameters investigated, it is found that pore size and surface porosity of PSf substrates were obviously altered with increasing polymer concentration in which higher concentration of polymer tended to produce smaller pore size and lower surface porosity, leading to reduction in pure water permeability. Results from ATR-IR spectra revealed that the specific functional group of PA was able to be detected over all PSf substrates regardless of the properties, confirming the successful formation of TFC membrane. Based on the AFM and FESEM analyses, it is reported that the physical properties of PA layer were changed using different PSf substrate properties, which were consistent with the change in water flux. Based on the FESEM pictures, it is found that the thickness of PA layer increased as the pores size decreased. The change in the membrane structural properties in particular pore size is found to portray significant contribution to the changes of formed PA layer. It was further postulated that PIP is supplied to the organic and aqueous phase interface by diffusion through the pores at the substrate skin layer from the pool of aqueous phase in the porous sublayer, and this is the rate controlling step for the PIP supply. Additionally, it was found that substrate roughness might not be the main factor governing the changes in TFC surface roughness. Overall, it is concluded that the TFC membrane made over substrate of 15 wt.% PSf concentration with an average pore size of 47.20 nm and 11.97% of surface porosity (SEM measurement) was the optimum membrane by taking into account both water permeability and salt rejection. The findings shown in this work have provided an answer as to why a PSf substrate made of 15 wt.% polymer concentration was widely employed as supporting membrane for TFC membrane fabrication, whether in the past or present.

Acknowledgments

The authors are grateful for the research financial support by the Ministry of Higher Education under Long-term Research Grant Scheme (Vot no. 4L803) and Universiti Teknologi Malaysia under Research University Grant Scheme (Vot no. Q.J.130000.7142.01H40). Author, N. Misdan thanks the sponsorship given by Ministry of Higher Education under MyBrain15 (MyPhD) scheme during her Ph.D. studies. The authors also gratefully thank Prof. Y. M. Lee in the WCU Department of Energy Engineering at Hanyang University (South Korea) for providing some instruments for the membrane characterization. Authors are also very grateful to Mr. D. W. Shin for performing the AFM characterizations.

References

[1] M. Ulbricht, Advanced functional polymer membranes, Polymer 47 (2006) 2217–2262.
[2] J. Cadotte, R. Forester, M. Kim, R. Petersen, T. Stocker, Nanofiltration membranes broaden the use of membrane separation technology, Desalination 70 (1988) 77–88.
[3] A. Rahimpour, M. Jahanshahi, N. Mortazavian, S.S. Madaeni, Y. Mansourpanah, Preparation and characterization of asymmetric polyethersulfone and thin-film composite polyamide nanofiltration membranes for water softening, Appl. Surf. Sci. 256 (2010) 1657–1663.
[4] R.S. Harisha, K.M. Hosamani, R.S. Keri, S.K. Nataraj, T.M. Aminabhavi, Arsenic removal from drinking water using thin film composite nanofiltration membrane, Desalination 252 (2010) 75–80.
[5] W.-J. Lau, A.F. Ismail, Polymeric nanofiltration membranes for textile dye wastewater treatment: preparation, performance evaluation, transport modelling, and fouling control — a review, Desalination 245 (2009) 321–348.
[6] L. Hu, S. Zhang, R. Han, X. Jian, Preparation and performance of novel thermally stable polyamide/PPENK composite nanofiltration membranes, Appl. Surf. Sci. 258 (2012) 9047–9053.
[7] A.F. Ismail, W.J. Lau, Influence of feed conditions on the rejection of salt and dye in aqueous solution by different characteristics of hollow fiber nanofiltration membranes, Desalin. Water Treat. 6 (2009) 281–288.
[8] R.J. Petersen, Composite reverse osmosis and nanofiltration membranes, J. Membr. Sci. 83 (1993) 81–150.
[9] W.J. Lau, A.F. Ismail, N. Misdan, M.A. Kassim, A recent progress in thin film composite membrane: a review, Desalination 287 (2012) 190–199.
[10] P.S. Singh, S.V. Joshi, J.J. Trivedi, C.V. Devmurari, A.P. Rao, P.K. Ghosh, Probing the structural variations of thin film composite RO membranes obtained by coating

polyamide over polysulfone membranes of different pore dimensions, J. Membr. Sci. 278 (2006) 19–25.
[11] H.I. Kim, S.S. Kim, Plasma treatment of polypropylene and polysulfone supports for thin film composite reverse osmosis membrane, J. Membr. Sci. 286 (2006) 193–201.
[12] A.K. Ghosh, E.M.V. Hoek, Impacts of support membrane structure and chemistry on polyamide–polysulfone interfacial composite membranes, J. Membr. Sci. 336 (2009) 140–148.
[13] G.Z. Ramon, M.C.Y. Wong, E.M.V. Hoek, Transport through composite membrane, part 1: is there an optimal support membrane? J. Membr. Sci. 415–416 (2012) 298–305.
[14] A. Prakash Rao, N.V. Desai, R. Rangarajan, Interfacially synthesized thin film composite RO membranes for seawater desalination, J. Membr. Sci. 124 (1997) 263–272.
[15] N.K. Saha, S.V. Joshi, Performance evaluation of thin film composite polyamide nanofiltration membrane with variation in monomer type, J. Membr. Sci. 342 (2009) 60–69.
[16] A. Soroush, J. Barzin, M. Barikani, M. Fathizadeh, Interfacially polymerized polyamide thin film composite membranes: preparation, characterization and performance evaluation, Desalination 287 (2012) 310–316.
[17] A.L. Ahmad, B.S. Ooi, Properties–performance of thin film composites membrane: study on trimesoyl chloride content and polymerization time, J. Membr. Sci. 255 (2005) 67–77.
[18] A.K. Ghosh, B.-H. Jeong, X. Huang, E.M.V. Hoek, Impacts of reaction and curing conditions on polyamide composite reverse osmosis membrane properties, J. Membr. Sci. 311 (2008) 34–45.
[19] I. Masselin, L. Durand-Bourlier, J.-M. Laine, P.-Y. Sizaret, X. Chasseray, D. Lemordant, Membrane characterization using microscopic image analysis, J. Membr. Sci. 186 (2001) 85–96.
[20] S. Zhao, Z. Wang, X. Wei, B. Zhao, J. Wang, S. Yang, S. Wang, Performance improvement of polysulfone ultrafiltration membrane using PANiEB as both pore forming agent and hydrophilic modifier, J. Membr. Sci. 385–386 (2011) 251–262.
[21] G.R. Guillen, T.P. Farrell, R.B. Kaner, E.M.V. Hoek, Pore-structure, hydrophilicity, and particle filtration characteristics of polyaniline–polysulfone ultrafiltration membranes, J. Mater. Chem. 20 (2010) 4621–4628.
[22] M. Khayet, C.Y. Feng, K.C. Khulbe, T. Matsuura, Preparation and characterization of polyvinylidene fluoride hollow fiber membranes for ultrafiltration, Polymer 43 (2002) 3879–3890.
[23] M.C. García-Payo, M. Essalhi, M. Khayet, Effects of PVDF-HFP concentration on membrane distillation performance and structural morphology of hollow fiber membranes, J. Membr. Sci. 347 (2010) 209–219.
[24] S. Singh, K.C. Khulbe, T. Matsuura, P. Ramamurthy, Membrane characterization by solute transport and atomic force microscopy, J. Membr. Sci. 142 (1998) 111–127.
[25] A. Bessières, M. Meireles, R. Coratger, J. Beauvillain, V. Sanchez, Investigations of surface properties of polymeric membranes by near field microscopy, J. Membr. Sci. 109 (1996) 271–284.
[26] A.K. Fritzsche, A.R. Arevalo, A.F. Connolly, M.D. Moore, V. Elings, C.M. Wu, The structure and morphology of the skin of polyethersulfone ultrafiltration membranes: a comparative atomic force microscope and scanning electron microscope study, J. Appl. Polym. Sci. 45 (1992) 1945–1956.
[27] M. Fathizadeh, A. Aroujalian, A. Raisi, Effect of lag time in interfacial polymerization on polyamide composite membrane with different hydrophilic sub layers, Desalination 284 (2012) 32–41.
[28] Y. Mansourpanah, S.S. Madaeni, A. Rahimpour, Fabrication and development of interfacial polymerized thin-film composite nanofiltration membrane using different surfactants in organic phase; study of morphology and performance, J. Membr. Sci. 343 (2009) 219–228.